Hindawi
Shock and Vibration
Volume 2019, Article ID 9573786, 8 pages
https://doi.org/10.1155/2019/9573786

Research Article

Numerical Simulation Study on Aeroacoustic Characteristics within Deformable Cavities

Ning Fangli[1,2], **Ning Shunshan**[1,2], **Zhang Changtong**[1,2] **and Liu Zhe**[1,2]

[1]*School of Mechanical Engineering, Northwestern Polytechnical University, Xi'an 710072, China*
[2]*Dongguan Sanhang Civil-Military Integration Innovation Institute, Dongguan 523808, China*

Correspondence should be addressed to Ning Fangli; ningfl@nwpu.edu.cn

Received 10 July 2018; Revised 10 December 2018; Accepted 23 December 2018; Published 7 March 2019

Academic Editor: M. I. Herreros

Cavity flow phenomena are encountered in many kinds of aviation vehicles. The flow-induced noise can easily cause structure resonance and fatigue damages. Therefore, the study on the mechanism and effective control methods of cavity noise are very important to engineering applications. A new active control method was proposed based on the deformable cavity in order to mitigate the cavity noise. Large eddy simulation (LES) and computational aeroacoustics (CAA) are combined to simulate a typical open cavity noise. The results show the first mode sound-pressure level (SPL) of tonal noise decreases gradually while the first mode frequency sharply jumps within a small range of the slant angle of the trailing and bottom wall. In addition, with the increase in the slant angle, the decrease of the first mode SPL of tonal noise at Mach 0.6 is more significant than that at Mach 0.85, but the increase of the first mode frequency at Mach 0.85 is more dramatical than that at Mach 0.6. The proposed method can not only reduce the first mode SPL obviously but also increase the first mode frequency dramatically, which makes it different from the natural frequency of the cavity structure and sequentially helps the cavity avoid fatigue damages from resonance.

1. Introduction

Flow over cavities has been widely studied during the last several years because of its practical and academic value. In aviation industry, cavity flow phenomena widely exist in different positions of aircraft, such as landing gear wheel wells of civil aircraft, the crevices in the surface of aircraft, and the weapon bays of modern combat aircraft. Especially for the modern combat aircraft, in order to reduce low radar cross section, the weapons are enclosed in weapon bays. However, the weapon bays can induce high self-sustaining oscillations which in turn can generate flow-induced noise arising from the cavities. The strong noise can exert severe damage on both sensitive parts of weapons and equipment within the cavities.

The control methods for cavity noise can be classified into passive control methods and active control methods. Passive control methods are to control cavity flow with geometric modifications and do not use external energy/momentum sources to control the flow. The common passive control methods include spoilers [1–5], fences [6, 7], stepped leading edge [8], vortex generators [9–12], leading edge serrations [13], passive resonant absorbers [14], passive venting system with a porous cavity floor [15], and geometric ramp trailing edges [16]. For instance, Vikramaditya and Kurian [16] experimentally studied the flow field over cavities with different slant angles of trailing walls. They observed a steep fall in amplitudes of oscillations in the case of the cavity with a slant angle of 45°, whereas for cavities with a slant angle of 30° and 15°, the amplitudes of oscillations increase. The passive control methods may demonstrate good performance at design flow conditions without much complexity but may lose efficacy at off-design conditions.

Active control methods employ external energy/momentum sources to control the cavity flow. The common active control methods include mass injection [17–20], slot blowing [21], microjet actuators [22], steady blowing [23, 24], plasma actuators [25–29], miniature fluidic actuators, speakers and resonant tubes [30], and oscillating

ramps and fences [31]. The active control methods can offer attractive noise suppression and can adjust control parameters according to different flow conditions. All of these active control methods have demonstrated control of cavity resonance under subsonic flow conditions, but only a few of these have been successful under supersonic-free stream conditions. In addition, Shaw [32] found that the acoustic feedback phenomenon and shear layer receptivity are very sensitive to the state of the boundary layer at the point of separation. Thus, the selection of the most effective active suppression concept should be based on a configuration as close to the full-scale one as possible.

In this work, a new active noise control method is proposed. A mechanism installed within the cavity is to construct a deformable cavity. Figure 1 shows the structures of the deformable cavity. In the deformable cavity, 1 is the fixed leading edge, 2 is the fixed leading wall, 3, 5, and 7 are the hinges, 4 is the bottom of the cavity, 6 is the trailing wall, and 8 is the trailing edge-contained sliders; sliders which can slide horizontally are placed in the guide rail 9 and structures indicated by 10 are the panels of both sides. Figure 2 shows a deformed situation of the cavity with the slant angle α of the trailing wall 6. The mechanism controls the deformation of the cavity by horizontally sliding the trailing edge 8 to control the change of the slant angle α of the trailing wall 6. At the same time, the bottom 4 is also slanted.

According to different flow conditions, the proposed method can adjust the slant angles of the bottom and trailing wall of the deformable cavity for suppressing the cavity noise. In order to study aeroacoustic characteristics within the deformable cavity under different flow conditions, a deformable cavity based on the geometry of M219 cavity [33–37] has been simulated in the work. The cavity flow and flow-induced noise are studied by large eddy simulation (LES) and computational aeroacoustics (CAA).

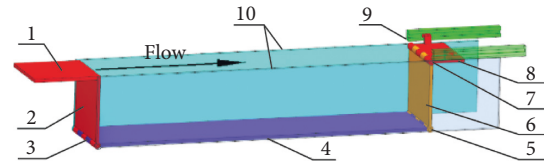

Figure 1: Three-dimensional schematic of a deformable cavity.

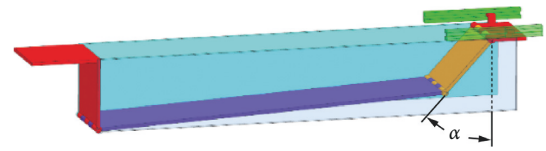

Figure 2: A deformed situation of the cavity with the slant angle α of the trailing wall 6.

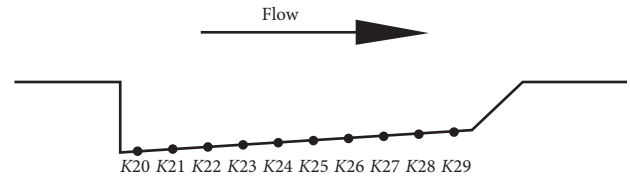

Figure 3: Monitoring points at the bottom of the deformable cavity.

Table 1: Positions of monitoring points.

Ceiling	Monitor	x/L
1	*K*20	0.05
2	*K*21	0.15
3	*K*22	0.25
4	*K*23	0.35
5	*K*24	0.45
6	*K*25	0.55
7	*K*26	0.65
8	*K*27	0.75
9	*K*28	0.85
10	*K*29	0.95

2. Computational Method

2.1. Cavity Configuration and Flow Parameters. In the present numerical simulation, the M219 cavity has dimensions of $L = 0.508$ m in length and $D = 0.1016$ m in depth, giving a ratio of $L : D = 5 : 1$. For comparison with the experimental results from the work of Chen et al. [34], the simulations were performed with free stream conditions of $M = 0.85$, $P = 62940$ Pa, and $T = 270.25$ K, and the Re (Reynolds number) based on the cavity length is 7,950,810. At the same time, the pressure across the cavity floor was monitored. These monitoring points are shown in Figure 3. It is shown that the monitoring locations are related to the length of the cavity in Table 1.

The inflow, outflow, and upper boundaries of the domain are applied with the pressure far-field conditions with $M = 0.85$, pressure $P = 62940$ Pa, and temperature $T = 270.25$ K. Adiabatic wall conditions are applied on the surface of the cavity walls.

2.2. Numerical Method. Because direct numerical simulation (DNS) is too expensive and unsteady Reynolds-averaged Naiver–Stokes (URANS) is unable to predict the unsteadiness within the cavity correctly, many computational fluid dynamics (CFD) researchers usually use LES to study various complex flow problems. The philosophy behind LES is to resolve the larger turbulence eddy scales, while a subgrid scale model is used to model the smaller turbulence eddy scales. Several recent efforts [38–41] that have applied LES to cavity flow have recently been published. Sinha et al. [38] found that engineering-oriented LES with modest grids provided a good representation of the interactions between narrow band, acoustic tones, and broadband, vortical turbulent structures. Levasseur et al. [39] simulated the cavity with the LES method in transonic and illustrated the ability of LES to capture the Rossiter frequencies at the cavity floor center. Thornber and Drikakis [40] simulated the deep cavity with the LES method and the results obtained showed that flow fields and sound-pressure

levels (SPLs) correlated very well with the experiment. Other LES studies have also attempted to model the important acoustics that occur in the supersonic regime over rectangular cavities [41], to develop a model to correlate the aspect ratio and Mach number. Therefore, the LES with the subgrid scale model is adopted to study the deformable cavity noise.

In LES, the motion is separated into the larger and the smaller turbulence eddies, and the separation is achieved by means of a low-pass filter. The filter function, $G(x, x')$, implied here is then as follows:

$$G(x, x') = \begin{cases} \dfrac{1}{V}, & x' \in V, \\ 0, & x' \notin V. \end{cases} \tag{1}$$

After filtering, a transient flow variable is divided into two parts:

$$\phi = \overline{\phi} + \phi', \tag{2}$$

where $\overline{\phi}$ is the mean component of the larger eddies, which can be calculated directly, and ϕ' is the component of the smaller eddies, which is represented with the subgrid scale model.

$\overline{\phi}$ is filtered as

$$\overline{\phi} = \int_D \phi G(x, x')\, dx', \tag{3}$$

where D is the flow domain, x' is a spatial term in the real flow domain, and x is a spatial coordinate of the larger eddies after filtering.

The formulas can be obtained with equation (3) and Navier–Stokes equations:

$$\frac{\partial \rho}{\partial t} + \frac{\partial (\rho \overline{u}_i)}{\partial x_i} = 0, \tag{4}$$

$$\frac{\partial \rho\, \overline{u}_i}{\partial y} + \frac{\partial \left(\rho \overline{u}_i \overline{u}_j\right)}{\partial x_j} = -\frac{\partial \overline{p}}{\partial x_i} + \frac{\partial \left(\mu \left(\partial \overline{u}_i / \partial x_j\right)\right)}{\partial x_i} - \frac{\partial \tau_{ij}}{\partial x_{ij}}, \tag{5}$$

where ρ is the fluid density, $\overline{u}_i$ is the mean flow speed, $\overline{p}$ is the mean pressure, μ is the viscosity coefficient of fluid molecules, and τ_{ij} is the subgrid stress tensor.

To solve equations (4) and (5), the basic SGS stress model [42, 43] is defined as

$$\tau_{ij} = \frac{1}{3}\tau_{kk}\delta_{ij} - 2\mu_t \overline{S}_{ij}, \tag{6}$$

where μ_t is the subgrid viscosity, δ_{ij} is the Kronecker delta (when $i = j$, $\delta_{ij} = 1$, $i \neq j$, and $\delta_{ij} = 0$), τ_{kk} is an isotropic part of the subgrid scale, and $\overline{S}_{ij}$ is the strain rate tensor of the subgrid scale.

Then, we can calculate

$$\mu_t = \left(C_s \Delta\right)^2 |\overline{S}|, \tag{7}$$

where $\overline{S}$ is the stretch rate tensor, $|\overline{S}| = \sqrt{2\overline{S}_{ij}\overline{S}_{ij}}$, $\Delta = \sqrt[3]{\Delta_x \Delta_y \Delta_z}$, Δ_i is the grid scale in the i direction, and C_s is the Smagorinsky constant.

In the work, LES with the dynamic Smagorinsky model (DSL) is performed. In the DSL subgrid model, the Smagorinsky constant C_s is dynamically computed based on the information provided by the resolved scales of motion. The gradient discrete scheme uses the least-squares cell-based gradient evaluation. The convective flux type adopts the Roe flux-difference splitting scheme. The inviscid convection term uses the second-order upwind scheme, and the viscous diffusion term uses the second-order central difference scheme. The time-dependent solution selects the second-order implicit, also known as the dual-time formulation.

The simulation includes the time histories of the pressure, $p(t)$, at locations $K20$–$K29$, respectively, which were recorded at each time step. The computation has been carried out for about 25,000 time steps, of which the first 5000 time steps have been discarded in the analysis of the pressure time series. The pressure oscillation is closely related to the sound resonance from the cavity. The recorded $p(t)$ has been used to compute the power spectral density (PSD) and the SPL. The SPLs are an indication of the intensity of noise generated in the cavity. The fast Fourier transform (FFT) has been used for $p(t)$ to compute the PSD. The SPL is then obtained from the calculated PSD, which is defined by

$$\mathrm{SPL}\,(\mathrm{dB}) = 10 \log\left(\frac{\mathrm{PSD}}{P_{\mathrm{ref}}^2}\right), \tag{8}$$

where $P_{\mathrm{ref}} = 2 \times 10^{-5}$ Pa is the value adopted as the minimum audible sound pressure variation.

2.3. Computational Mesh. The computational domain consists of the cavity region itself and the external flow region. Structured grids are adopted, and the grid structure of the deformable cavity used in this work is shown in Figure 4. The fineness of the grid structure near the wall is evaluated by y^+:

$$y^+ = \frac{\Delta y \rho u_\tau}{\mu} = \frac{\Delta y}{\nu}\sqrt{\frac{\tau_w}{\rho}}, \tag{9}$$

where Δy is the initial grid spacing normal to the wall, ρ is the fluid density, u_τ is the wall friction velocity, τ_w is the wall shear stress, and μ is the fluid viscosity. In the wall normal direction, the mesh is stretched according to smooth stretching ratios. In terms of wall units, y^+ near the wall in the wall normal direction is about $y^+ \approx 1$. In order to verify the independence of the grid structure, three grid structures were simulated, which were coarse, medium, and fine grid structures. The cell numbers of these are 65,000, 106,000, and 154,000, respectively. The fine grid structure is shown in Figure 4. Since the cavity itself is the main research object of the aerodynamic noise problem, the differences between various grid structures are mainly embodied in the different cell numbers of the cavity itself. The cell numbers of coarse, medium, and fine grid structures are 260×140, 380×200, and 500×260, respectively. After simulations, we found that the differences of the results among the three grid structures are very small, and the results of fine grid structures are the

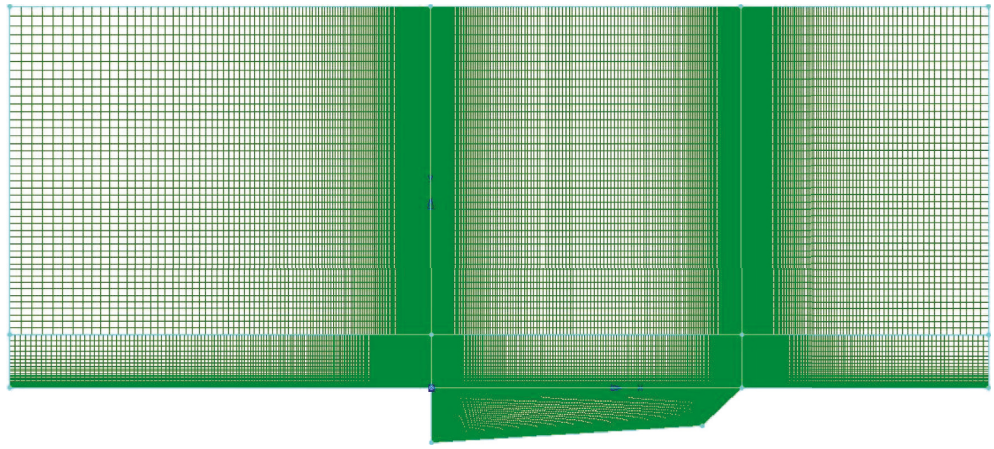

Figure 4: 2D fine grid structure of deformable cavity.

best compared with the experimental results. Therefore, we adopted the fine grid structure in this work.

The Courant number is given by the following equation:

$$C_o = \max\left(\frac{|u|}{\Delta x}\right)\Delta t, \tag{10}$$

where u is the free stream velocity, Δt is the time step, and Δx is the length of the grid in the direction of velocity. During the simulation of cavity noise, it is necessary to ensure that the Courant number is less than or equal to 1 in the entire flow field in order to achieve numerical stability and time calculation accuracy, so the time step is $\Delta t \approx 2 \times 10^{-5}$ s based on the grid structure we adopted.

2.4. Validations. Figure 5 illustrates the SPL, in decibels, predicted with LES with DSL subgrid model and compared with the experimental and simulation data obtained from Chen et al. [34]. The data represent the pressure points at *K*29, located near the trailing wall. The magnitude of SPL is sufficiently predicted, and the resonance frequencies clearly result from the computed spectrum. Among the simulation results of three grid structures, the magnitude of SPL of fine grid structure is the closest to the experimental results, so the fine grid structure is adopted in the paper.

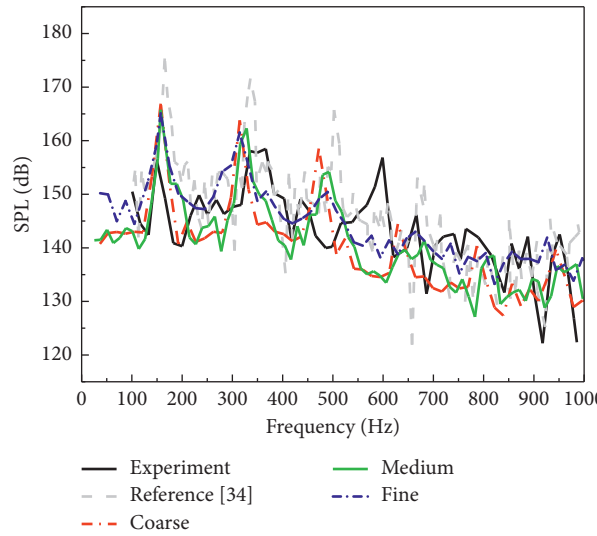

Figure 5: Spectrum of *K*29.

Figure 6: Sketch map for the depth d.

2.5. Volume Changes of Deformable Cavity. In Figure 6, D is the depth of the cavity near the leading wall, d is the depth of the cavity near the trailing wall, and α is the slant angle of the trailing wall. By calculation, when the bottom and trailing walls are on a straight line, α takes the maximum value of 80.406°. In Figure 7, we can see that the space of cavity near the trailing wall is gradually compressed as α gradually increases. When α increases to 60°, d has been reduced to half of D. Considering the practical engineering applications, the range of α is limited in the range of $0° \le \alpha \le 60°$ in this work.

α is divided into sixteen equal parts. That is, α gradually increases from 0° to 60°. Then, we establish the deformable cavity model and grid structures, respectively.

3. Results and Analysis

3.1. Flow Field Analysis. The property of the unsteady flow field is closely related to the sound resonance from the cavity, so the instantaneous vorticity contours of the flow field was observed. Figure 8 shows the comparison of instantaneous vorticity contours of the rectangle cavity ($\alpha = 0°$) at $t = 4/6T$ and deformable cavity ($\alpha = 60°$) at $t' = 4/6T'$. Figure 9 shows the comparison of instantaneous vorticity contours of the rectangle cavity ($\alpha = 0°$) at $t = 5/6T$ and deformable cavity ($\alpha = 60°$) at $t' = 5/6T'$. In Figures 8 and 9, t and t' are the current time of the instantaneous vorticity contours. T is the period related to the first Rossiter frequency of the rectangle

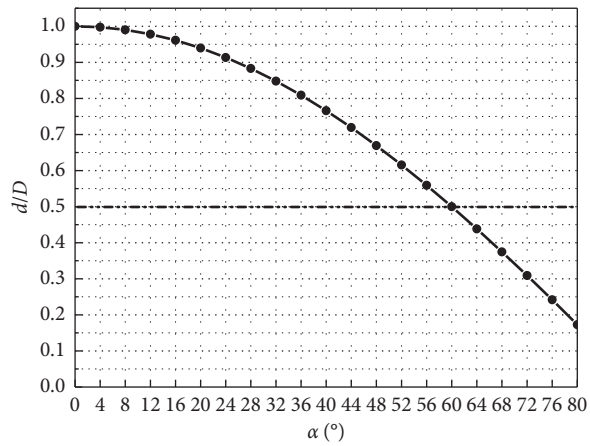

Figure 7: The depth d as a function of the slant angle α.

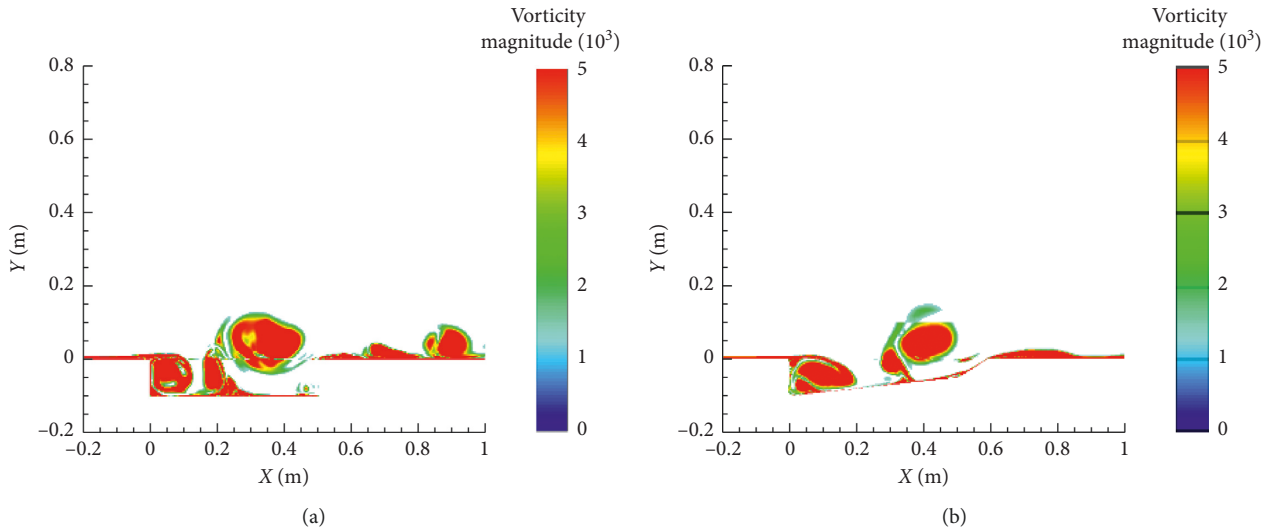

Figure 8: Comparison of the instantaneous vorticity contours of the rectangle cavity ($\alpha = 0°$) at $t = 4/6T$ (a) and deformable cavity ($\alpha = 60°$) at $t' = 4/6T'$ (b).

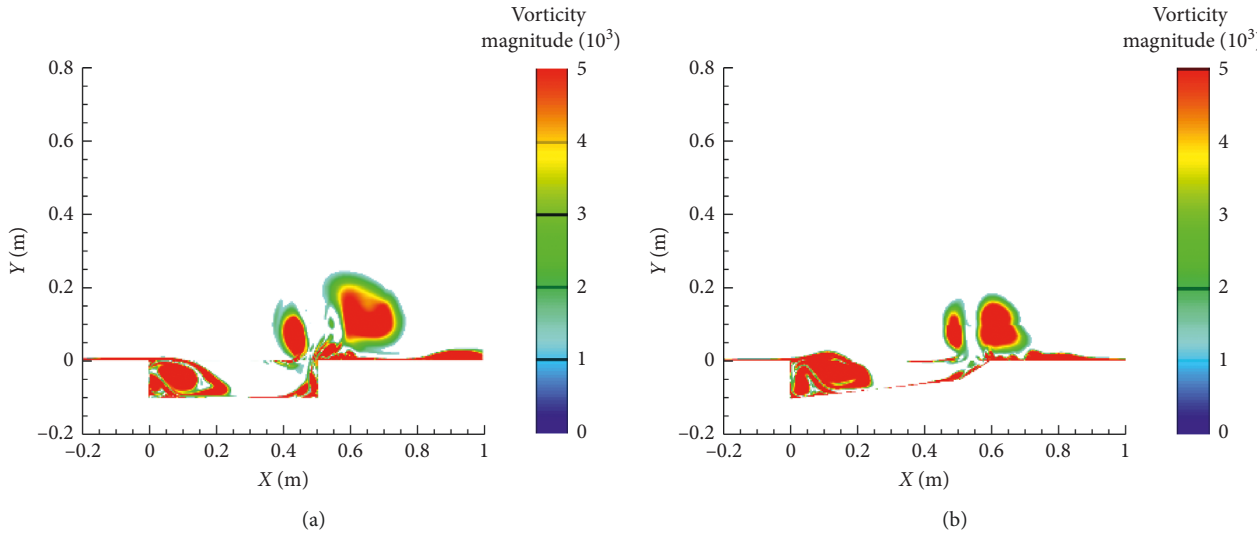

Figure 9: Comparison of the instantaneous vorticity contours of the rectangle cavity ($\alpha = 0°$) at $t = 5/6T$ (a) and deformable cavity ($\alpha = 60°$) at $t' = 5/6T'$ (b).

cavity. T' is the period related to the first Rossiter frequency of the deformable cavity with $\alpha = 60^{\circ}$. Compared with the rectangle cavity flow field, the flow field of deformable cavity with $\alpha = 60^{\circ}$ has the following differences:

(i) In Figure 8, we can clearly find that the vortices separating from the leading edge in the deformable cavity ($\alpha = 60^{\circ}$) are smaller than those in the rectangular cavity, which can make the impingement force between the vortices and trailing edge decrease in the deformable cavity.

(ii) When $\alpha = 60^{\circ}$, the corner of the trailing wall becomes more blunt than that of the rectangle cavity, which can also make the impingement force decrease and make the cavity noise radiate to exterior greatly.

(iii) In Figures 8(b) and 9(b), the vortices gradually upraised from the leading edge to the trailing edge. In Figure 8(b), the vortices are almost above the trailing edge. In Figure 9(b), most of the vortice forms are also clearly discernible after impingement. The above phenomena are quite different from that shown in Figures 8(a) and 8(b).

In view of the three points above, we can conclude that the flow field of the deformable cavity has been improved greater than that of the rectangle cavity. Taking into account the cavity noise mechanism of impingement, the strong noise environment in the original rectangle cavity may be improved inevitably.

3.2. Sound Field Analysis. Figure 10 shows the comparison of the first mode SPL of tonal noise at *K*29 when Mach is 0.6 and 0.85, respectively. The first mode SPL of tonal noise at *K*29 decreases as α gradually increases at Mach 0.6 and Mach 0.85. When Mach is 0.6, the first mode SPL of tonal noise at *K*29 decreases 10.43 dB at $\alpha = 60^{\circ}$, but when Mach is 0.85, the first mode SPL of tonal noise at *K*29 decreases 6.02 dB at $\alpha = 60^{\circ}$. It is obvious that the decrease of the first mode SPL of tonal noise at Mach 0.6 is more significant than that at Mach 0.85 as α gradually increases.

In the practical engineering applications, the cavities of aircraft are usually used to transport the weapons and other equipment. Therefore, we should ensure that the cavity has enough space for carriage. For this reason, when we select the slant angle of the trailing wall α, we should fully consider α and its potential interaction with the space of cavity. In addition, we found an interesting phenomenon that not only the SPL of the first mode of the tonal noise decreases significantly but also the frequency of the first mode of the tonal noise increases dramatically when the deformation of the cavity has changed.

Figure 11 shows the comparison of the first mode frequency of tonal noises at *K*29 when Mach is 0.6 and 0.85, respectively. When Mach is 0.6, the first mode frequency of tonal noise at *K*29 remains 128.20 Hz with the increase of α from 0° to 33°(rectangular cavity at $\alpha = 0^{\circ}$), then increases dramatically to 174.85 Hz as α increases from 33° to 34°, and lastly remains 174.85 Hz as α increases from 34° to 60°.

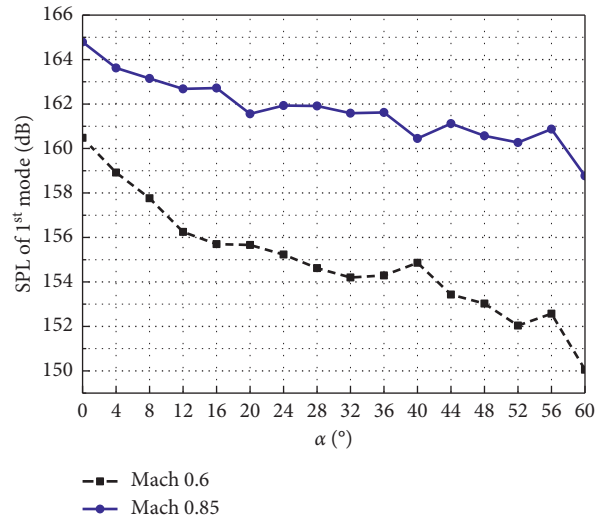

Figure 10: Comparison of the first mode SPLs of tonal noise at *K*29.

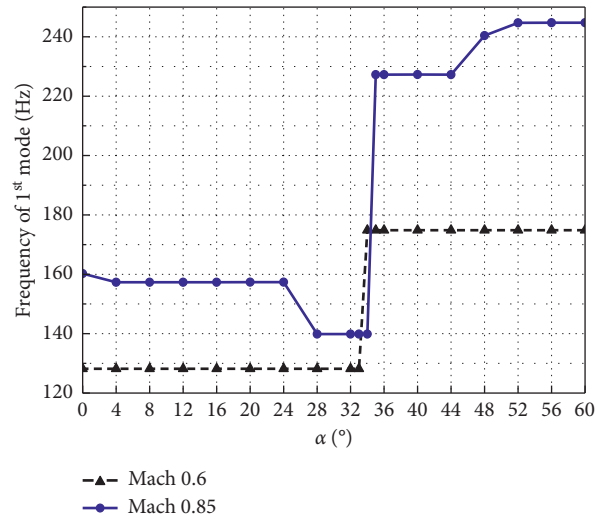

Figure 11: Comparison of the first mode frequencies of tonal noise at *K*29.

Finally, the first mode frequency of the tonal noise increases 46.65 Hz. When Mach is 0.85, the first mode frequency first decreases slightly from 160.25 Hz and then remains 157.33 Hz with the increase of α from 0° to 24°; then it decreases to 139.85 Hz with the increase of α from 24° to 28° and remains 139.85 Hz with the increase of α from 28° to 34°; later, it increases dramatically to 227.26 Hz with the increase of α from 34° to 35° and remains 227.26 Hz with the increase of α from 35° to 44°; then, it increases to 244.74 Hz with the increase of α from 44° to 52° and remains 244.74 Hz with the increase of α from 52° to 60°. Finally, the first mode frequency of tonal noise increases 84.49 Hz. It is obvious that the increase of the first mode frequency of tonal noise at Mach 0.85 is more dramatical than that at Mach 0.6.

In fact, the dramatical increase of the first mode frequency will make the sound resonance frequency different from the natural frequency of cavity structure, which can

mitigate the damage of resonance to the cavity structure. The phenomenon of dramatical increase in the resonance frequency is also found by Rowly et al. [44]. They concluded that the resonance frequency decreases as L (the length of cavity) gradually increases, but once a critical value of L is reached, the frequency jumps up, as the cavity switches to a high mode. According to their conclusion, the phenomenon of dramatical increase in the first mode frequency that appeared in the deformable cavity can be explained as follows: the actual effective length of cavity has changed due to the change of the cavity shape. When the actual effective length is changed to a critical value, the first mode frequency increases dramatically.

In the practical engineering applications, the SPL and frequency of first mode can be fully considered to the selection of α. α should be located in the range where the first mode frequency has increased dramatically. At the same time, we can select α to make the first mode SPL reduce greatly according to the actual needs of the cavity volume.

4. Conclusions

In this work, the numerical simulation of LES is used to verify the feasibility of the proposed active control method for cavity noise at Mach 0.6 and 0.85. The following conclusions are obtained through comprehensive analysis:

(i) When Mach is 0.85, the first mode SPL of tonal noise at $K29$ decreases as α gradually increases, and the maximum reduction is 6.02 dB. When Mach is 0.6, the first mode SPL of tonal noise at $K29$ also decreases as α gradually increases, but the maximum reduction is 10.43 dB. This shows that the decrease of the first mode SPL of tonal noise at Mach 0.6 is more significant than that at Mach 0.85 as α gradually increases. The decrease of the first mode SPL of tonal noise has an important positive effect on improving the noise environment and protecting the devices within cavity.

(ii) The first mode frequency sharply jumps within a small range of the slant angle α of the trailing wall. When Mach is 0.85, the first mode frequency of tonal noise at $K29$ increases 87.41 Hz dramatically with the increase of α from 34° to 35°. When Mach is 0.6, the first mode frequency of tonal noise at $K29$ increases 46.65 Hz dramatically with the increase of α from 33° to 34°. Obviously, the increase of the first mode frequency of tonal noise at Mach 0.85 is more dramatical than that at Mach 0.6 as α gradually increases. The dramatical increase of the first mode frequency of tonal noise can make the sound resonance frequency different from the natural frequency of cavity structure, which can mitigate the damage of resonance to the cavity structure.

Data Availability

The data used to support the findings of this study are available from the corresponding author upon request.

Conflicts of Interest

The authors declare that they have no conflicts of interest.

Acknowledgments

This work was supported by the National Science Foundation of China (nos. 51675425 and 51375385), Shaanxi Provincial Natural Science Foundation of China (no. 2016JZ013), and Dongguan Social Science and Technology Development (Key) Project (no. 20185071021600). The authors also thank Juan Wei for revising the paper and polishing English.

References

[1] S. Moon, S. Gai, H. Kleine, and A. Neely, "Supersonic flow over straight shallow cavities including leading and trailing edge modifications," in *Proceedings of 28th AIAA Applied Aerodynamics Conference*, vol. 4687, Chicago, IL, USA, June-July 2010.

[2] A. J. Saddington, V. Thangamani, and K. Knowles, "Comparison of passive flow control methods for a cavity in transonic flow," *Journal of Aircraft*, vol. 53, no. 5, pp. 1439–1447, 2016.

[3] A. J. Saddington, K. Knowles, and V. Thangamani, "Scale effects on the performance of sawtooth spoilers in transonic rectangular cavity flow," *Experiments in Fluids*, vol. 57, no. 1, p. 2, 2016.

[4] L. Xie, J. Ai, H. Feng et al., "The study of cavity flow and leading edge spoiler based on DES," in *Proceedings of 47th AIAA Fluid Dynamics Conference*, vol. 3130, Denver, CO, USA, June 2017.

[5] K. Luo, W. Zhe, Z. Xiao, and S. Fu, "Improved delayed detached-eddy simulations of sawtooth spoiler control before supersonic cavity," *International Journal of Heat and Fluid Flow*, vol. 63, pp. 172–189, 2017.

[6] L. S. Ukeiley, M. K. Ponton, J. M. Seiner, and B. Jansen, "Suppression of pressure loads in cavity flows," *AIAA Journal*, vol. 42, no. 1, pp. 70–79, 2004.

[7] K. Anupindi and R. D. Sandberg, "Implementation and evaluation of an embedded LES-RANS solver," *Flow, Turbulence and Combustion*, vol. 98, no. 3, pp. 697–724, 2017.

[8] D. G. MacManus and D. S. Doran, "Passive control of transonic cavity flow," *Journal of Fluids Engineering*, vol. 130, no. 6, article 064501, 2008.

[9] S. Perng, D. Dolling, S. Perng, and D. Dolling, "Attenuation of pressure oscillations in high speed cavity flow through geometry changes," in *Proceedings of 28th Fluid Dynamics Conference*, vol. 1802, Snowmass Village, CO, USA, June 1997.

[10] J. C. Lin, "Review of research on low-profile vortex generators to control boundary-layer separation," *Progress in Aerospace Sciences*, vol. 38, no. 4-5, pp. 389–420, 2002.

[11] P. R. Ashill, J. L. Fulker, and K. C. Hackett, "A review of recent developments in flow control," *The Aeronautical Journal*, vol. 109, no. 1095, pp. 205–232, 2005.

[12] A. Omer and A. Mohany, "The effect of high frequency vortex generator on the acoustic resonance excitation in shallow rectangular cavities," *Canadian Acoustics*, vol. 42, no. 3, 2014.

[13] S. L. Gai, H. Kleine, and A. J. Neely, "Supersonic flow over a shallow open rectangular cavity," *Journal of Aircraft*, vol. 52, no. 2, pp. 609–616, 2014.

[14] D. A. Roberts, D. G. MacManus, R. A. Johnson, J. E. Grove, T. J. Birch, and R. A. Chaplin, "Passive attenuation of modal

cavity aeroacoustics under supersonic and transonic conditions," *AIAA Journal*, vol. 53, no. 7, pp. 1861–1877, 2014.

[15] F. J. Wilcox, "Passive venting system for modifying cavity flowfields at supersonicspeeds," *AIAA Journal*, vol. 26, no. 3, pp. 374–376, 1988.

[16] N. S. Vikramaditya and J. Kurian, "Effect of aft wall slope on cavity pressure oscillations in supersonic flows," *The Aeronautical Journal*, vol. 113, no. 1143, pp. 291–300, 2009.

[17] A. D. Vakili and C. Gauthier, "Control of cavity flow by upstream mass-injection," *Journal of Aircraft*, vol. 31, no. 1, pp. 169–174, 1994.

[18] S. Arunajatesan, C. Kannepalli, N. Sinha et al., "Suppression of cavity loads using leading-edge blowing," *AIAA Journal*, vol. 47, no. 5, pp. 1132–1144, 2009.

[19] W. Li, T. Nonomura, and K. Fujii, "Mechanism of controlling supersonic cavity oscillations using upstream mass injection," *Physics of Fluids*, vol. 25, no. 8, article 086101, 2013.

[20] Y. Zhang, N. Arora, Y. Sun, L. N. Cattafesta, K. Taira, and L. S. Ukeiley, "Suppression of cavity oscillations via three-dimensional steady blowing," in *Proceedings of 45th AIAA Fluid Dynamics Conference*, vol. 3219, Dallas, TX, USA, June 2015.

[21] T. Lusk, L. Cattafesta, and L. Ukeiley, "Leading edge slot blowing on an open cavity in supersonic flow," *Experiments in Fluids*, vol. 53, no. 1, pp. 187–199, 2012.

[22] M. Y. Ali, J. T. Solomon, J. Gustavsson, R. Kumar, and F. Alvi, "Control of resonant flow inside a supersonic cavity using high bandwidth pulsed micro-actuators," in *Proceedings of 48th AIAA Aerospace Sciences Meeting Including the New Horizons Forum and Aerospace Exposition*, vol. 1198, Orlando, FL, USA, January 2010.

[23] L. Ukeiley, M. Sheehan, F. Coiffet, F. Alvi, S. Arunajatesan, and B. Jansen, "Control of pressure loads in geometrically complex cavities," *Journal of Aircraft*, vol. 45, no. 3, pp. 1014–1024, 2008.

[24] B. George, L. S. Ukeiley, L. N. Cattafesta et al., "Control of three-dimensional cavity flow using leading-edge slot blowing," in *Proceedings of 53rd AIAA Aerospace Sciences Meeting*, vol. 1059, Kissimmee, FL, USA, January 2015.

[25] X. Huang and X. Zhang, "Plasma actuators for noise control," *International Journal of Aeroacoustics*, vol. 9, no. 4-5, pp. 679–703, 2010.

[26] A. de Jong and H. Bijl, "Corner-type plasma actuators for cavity flow-induced noise control," *AIAA Journal*, vol. 52, no. 1, pp. 33–42, 2013.

[27] K. Yugulis, S. Hansford, J. W. Gregory, and M. Samimy, "Control of high subsonic cavity flow using plasma actuators," *AIAA Journal*, vol. 52, no. 7, pp. 1542–1554, 2014.

[28] N. J. Webb and M. Samimy, "Supersonic cavity control using plasma actuators," in *Proceedings of 53rd AIAA Aerospace Sciences Meeting*, vol. 1961, Kissimmee, FL, USA, January 2015.

[29] N. Webb and M. Samimy, "Control of supersonic cavity flow using plasma actuators," *AIAA Journal*, vol. 55, no. 10, pp. 3346–3355, 2017.

[30] M. Samimy, M. Debiasi, E. Caraballo et al., "Feedback control of subsonic cavity flows using reduced-order models," *Journal of Fluid Mechanics*, vol. 579, pp. 315–346, 2007.

[31] R. L. Sarno and M. E. Franke, "Suppression of flow-induced pressure oscillations in cavities," *Journal of Aircraft*, vol. 31, no. 1, pp. 90–96, 1994.

[32] L. Shaw, "Active control for cavity acoustics," in *Proceedings of 4th AIAA/CEAS Aeroacoustics Conference*, vol. 2347, Toulouse, France, June 1998.

[33] F. Mendonça, R. Allen, J. de Charentenay, and D. Kirkham, "CFD prediction of narrowband and broadband cavity acoustics at $M = 0.85$," in *Proceedings of 9th AIAA/CEAS Aeroacoustics Conference and Exhibit*, vol. 3303, Hilton Head Island, SC, USA, May 2003.

[34] X. Chen, N. D. Sandham, and X. Zhang, "Cavity flow noise predictions," Final Report for MSTARR DARP School of Engineering Sciences, University of Southampton, Southampton, UK, 2007.

[35] S. V. Babu and G. N. Barakos, "Prediction of acoustics of transonic cavities using DES and SAS," in *Proceedings of 49th International Symposium of Applied Aerodynamics: Aerodynamics and Environment*, Lille, France, March 2014.

[36] L. Xiao, Z. Xiao, Z. Duan, and S. Fu, "Improved-delayed-detached-eddy simulation of cavity-induced transition in hypersonic boundary layer," *International Journal of Heat and Fluid Flow*, vol. 51, pp. 138–150, 2015.

[37] S. V. Babu, G. Zografakis, and G. N. Barakos, "Evaluation of scale-adaptive simulations for transonic cavity flows," in *Proceedings of Progress in Hybrid RANS-LES Modelling*, pp. 433–444, Springer, College Station, TX, USA, March 2015.

[38] N. Sinha, S. Dash, N. Chidambaram, and D. Findlay, "A perspective on the simulation of cavity aeroacoustics," in *Proceedings of 36th AIAA Aerospace Sciences Meeting and Exhibit*, vol. 286, Reno, NV, USA, 1998.

[39] V. Levasseur, P. Sagaut, M. Mallet, and F. Chalot, "Unstructured large eddy simulation of the passive control of the flow in a weapon bay," *Journal of Fluids and Structures*, vol. 24, no. 8, pp. 1204–1215, 2008.

[40] B. Thornber and D. Drikakis, "Implicit large-eddy simulation of a deep cavity using high-resolution methods," *AIAA Journal*, vol. 46, no. 10, pp. 2634–2645, 2008.

[41] T. Handa and M. Masuda, "On the jump in the frequency of acoustic oscillations in supersonic flows over rectangular cavity," *Physics of Fluids*, vol. 21, no. 2, article 026102, 2009.

[42] J. Smagorinsky, "General circulation experiments with the primitive equations: I. The basic experiment," *Monthly Weather Review*, vol. 91, no. 3, pp. 99–164, 1963.

[43] A. Mochida, S. Murakami, Y. Tominaga, and H. Kobayashi, "Comparison between standard and dynamic type of smagorinsky SGS model: large eddy simulation of turbulent vortex shedding flow past 2D square cylinder using dynamic SGS model (Part 1)," *Journal of Architecture and Planning (Transactions of AIJ)*, vol. 61, no. 479, pp. 41–47, 1996.

[44] C. Rowley, T. Colonius, and R. Murray, "POD based models of self-sustained oscillations in the flow past an open cavity," in *Proceedings of 6th Aeroacoustics Conference and Exhibit*, vol. 1969, Lahaina, HI, USA, 2000.